Bio-Design and Manufacturing (2024) 7:88–103
https://doi.org/10.1007/s42242-023-00262-2

RESEARCH ARTICLE

Semi-implantable device based on multiplexed microfilament electrode cluster for continuous monitoring of physiological ions

Shuang Huang[1,2] · Shantao Zheng[1] · Mengyi He[1] · Chuanjie Yao[1] · Xinshuo Huang[1] · Zhengjie Liu[1] · Qiangqiang Ouyang[3] · Jing Liu[3] · Feifei Wu[1,4] · Hang Gao[5] · Xi Xie[1,2,3] · Hui-jiuan Chen[1]

Received: 20 January 2023 / Accepted: 7 November 2023 / Published online: 19 December 2023

Abstract

Modern medicine is increasingly interested in advanced sensors to detect and analyze biochemical indicators. Ion sensors based on potentiometric methods are a promising platform for monitoring physiological ions in biological subjects. Current semi-implantable devices are mainly based on single-parameter detection. Miniaturized semi-implantable electrodes for multiparameter sensing have more restrictions on the electrode size due to biocompatibility considerations, but reducing the electrode surface area could potentially limit electrode sensitivity. This study developed a semi-implantable device system comprising a multiplexed microfilament electrode cluster (MMEC) and a printed circuit board for real-time monitoring of intra-tissue K^+, Ca^{2+}, and Na^+ concentrations. The electrode surface area was less important for the potentiometric sensing mechanism, suggesting the feasibility of using a tiny fiber-like electrode for potentiometric sensing. The MMEC device exhibited a broad linear response (K^+: 2–32 mmol/L; Ca^{2+}: 0.5–4 mmol/L; Na^+: 10–160 mmol/L), high sensitivity (about 20–45 mV/decade), temporal stability (>2 weeks), and good selectivity (>80%) for the above ions. In vitro detection and in vivo subcutaneous and brain experiment results showed that the MMEC system exhibits good multi-ion monitoring performance in several complex environments. This work provides a platform for the continuous real-time monitoring of ion fluctuations in different situations and has implications for developing smart sensors to monitor human health.

Graphic abstract

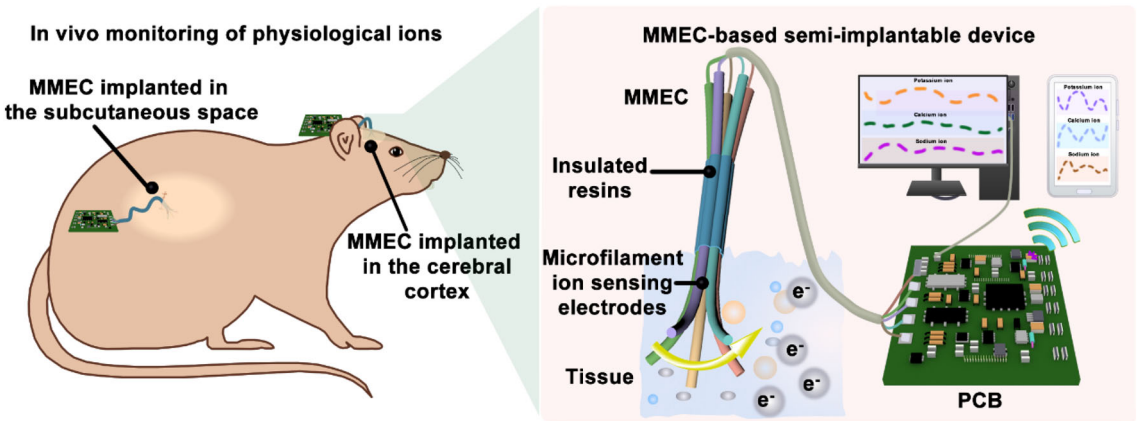

Keywords Multiplexed microfilament electrode cluster · Physiological ion sensing · Subcutaneous and brain experiment · Wearable platform for multi-ion detection · Continuous real-time monitoring system

Extended author information available on the last page of the article

Introduction

Advances in biomedical sensing technology are important and directly related to developing new diagnostic and therapeutic instruments [1, 2]. Traditional biosensing is based on in vitro laboratory testing of blood, urine, and biopsy samples [3]. Moreover, detecting ion concentrations in the body is crucial for assessing human health because it has implications for human activity, organ pathology, and metabolism studies in certain underlying diseases [4]. Ion monitoring in human tissues using interstitial fluid (ISF) samples allows an accurate assessment of the ionic status of the tissue microenvironment and avoids pain and inconvenience by blood tests [5]. Furthermore, monitoring of physiological ions, such as K^+, Ca^{2+}, and Na^+, has made it possible to record the chemical activity of ion channels in the brain, deepening the understanding of daily brain activity and pathophysiological processes [6–9]. For example, Zhao et al. implanted electrochemical physiological microarrays in rat brains to study ion dynamics in the deep brain of freely moving rats during seizures [4]. Wang et al. reported ion-selective electrode arrays that could detect Na^+ and K^+ concentrations in subcutaneous ISF in patients with hypernatremia and hypokalemia in real time to obtain timely physiological information to assist treatment [7].

Implantable/wearable sensing devices have emerged to obtain more accurate, stable, and continuous information about living organisms [10–12]. The maturation of wearable [13–15] and implantable [16, 17] devices has made online sensing of information within living bodies possible. Moreover, semi-implantable bioelectronics [18] meets the growing technological need for precisely detecting or regulating biological activities. It provides an ideal platform for integrating complex functional electronic devices externally. Semi-implantable sensing devices have significantly progressed over the past decades, especially semi-implantable electrodes, such as continuous glucose monitoring electrodes [19, 20] that monitor subcutaneous biological signals [21] and brain electrodes [22] that monitor brain signals. However, current semi-implantable devices for monitoring subcutaneous markers are primarily used for detecting glucose, whereas brain electrodes are primarily used for monitoring electroencephalographic signals [23, 24]. Implantable devices for biochemical analyte detection in the brain include microdialysis sampling probes, a commonly used technique for real-time, minimally invasive sampling of extracellular cerebral fluid. However, these probes can rarely detect biomarkers continuously with short intervals and possess low spatial resolution [25]. Moreover, noninvasive wearable devices [26] are incapable of real-time, in situ online detection of physiological ions in vivo due to a skin barrier. Therefore, developing a semi-implantable device for continuous subcutaneous/intracerebral monitoring of ions is highly desirable for the in vivo detection of biochemical substances.

Given the complexity of the fluid environment in the body, simultaneous and real-time detection of multiple biomarkers is critical, requiring the construction of multiparameter sensing systems to ensure the diversity and accuracy of measurements [26, 27]. Multiparameter sensors have high detection efficiency for tracking multiple analytes in parallel at a time, making them an ideal choice for simultaneous biomedical sensing of various components [28]. Concurrently, the simultaneous monitoring and analysis of multiple parameters allow for a deeper understanding and precise control of in vivo health conditions [29]. For example, a fully integrated wearable sensor array for multianalyte sensing was developed by Gao et al. [30]. However, most multiparameter sensing electrodes are based on planar electrodes applied to the skin surface for sweat [31–33], saliva [34], tear [35], and urine [36] analysis, and sweat analysis is the most commonly used method [37–39]. For semi-implantable devices, single-parameter detectors are still the majority, with only a few reported devices capable of simultaneously testing multiple parameters in vivo. Implantable devices prepared using flexible polyimide (PI) substrates can be employed for in situ multifunctional sensing within the body [40]. However, flexible PI substrates encompassing multiple functionalities while ensuring sensing performance typically exhibit larger dimensions. These large-sized planar sensing structures hinder the mobility of dynamic tissues such as muscles. It leads to instability at the interface between the device and the tissue. Consequently, the fabrication of small-sized multifunctional sensors significantly reduces tissue damage and hinders muscle motion [41]. Among these, the small size and excellent flexibility of fiber-like electrodes position them as potential candidates for implantable electrodes. However, downsizing semi-implantable sensing electrodes results in decreased electrode surface area and higher fabrication complexities associated with their three-dimensional structure. These factors can lead to compromised electrode performance, such as reduced sensing sensitivity and a narrowed linear range. In contrast, miniaturized semi-implantable sensing electrodes have more restrictions on the electrode size to ensure biocompatibility, but reducing the electrode surface area is likely to limit the electrode performance, such as sensing sensitivity and linear range.

This study developed a multiplexed microfilament electrode cluster (MMEC)-based semi-implantable device system for real-time and in situ monitoring of K^+, Ca^{2+}, and Na^+ concentrations in the subcutaneous and intracranial environment. MMEC used well-performing Au microfilaments as a flexible electrode array to sense K^+, Ca^{2+}, and Na^+

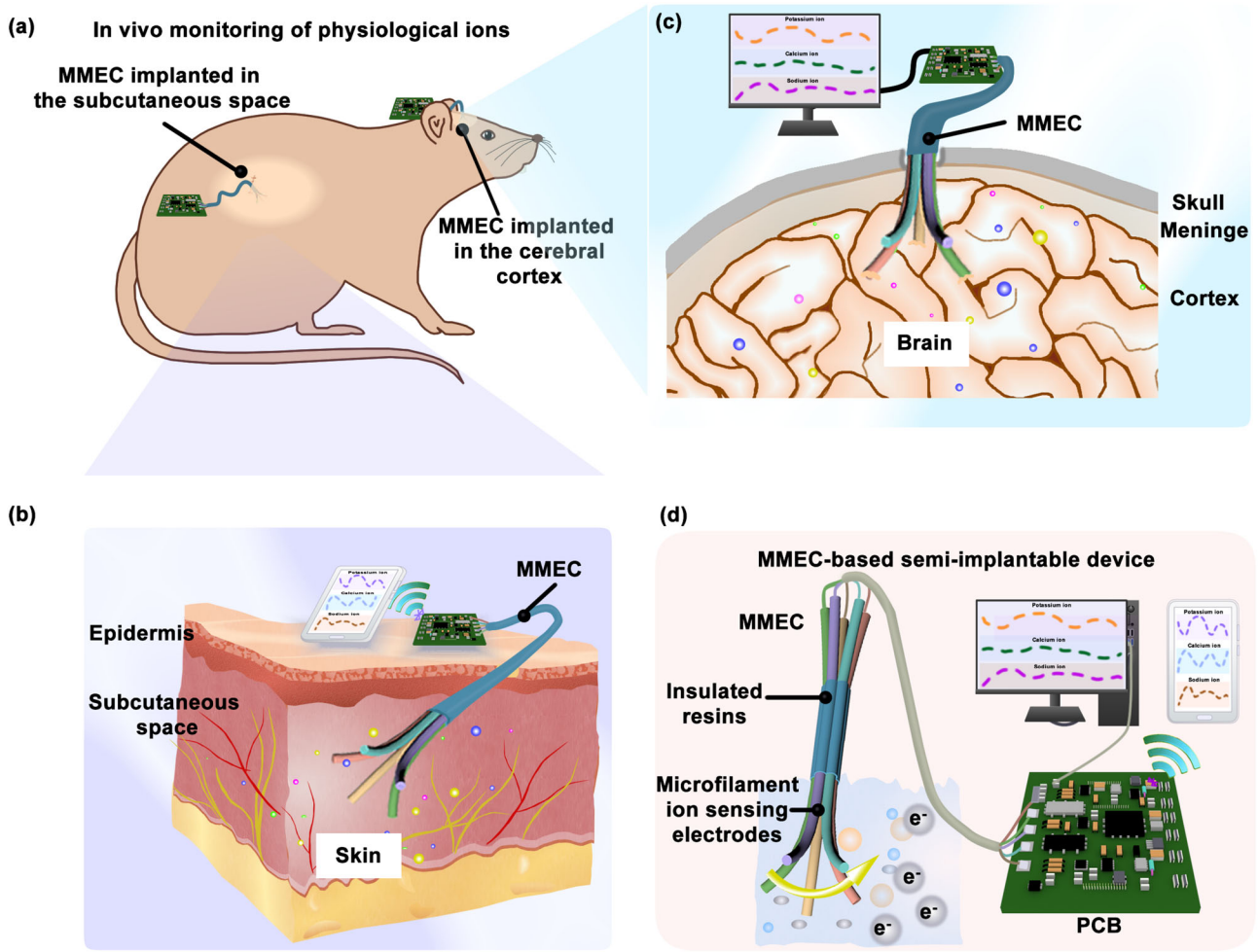

Fig. 1 Schematic diagram of MMEC for in vivo continuous monitoring of three types of physiological ions. **a** Schematic diagram of the fixation of the MMEC device during in vivo detection, where the MMEC was implanted in the **b** subcutaneous space on the back or **c** cerebral cortex of the rat for continuous monitoring of real-time ion concentrations in tissues. **d** Schematic diagram of the MMEC-based semi-implantable system. The MMEC device was connected to a customized PCB for simultaneous monitoring of Na^+, K^+, and Ca^{2+} concentrations, and the PCB transmitted the monitored potentiometric signals to a computer or mobile terminal. MMEC: multiplexed microfilament electrode cluster; PCB: printed circuit board

based on open-circuit potentiometry to measure ion concentrations (Fig. 1). The Au microfilament electrode was modified using poly(3,4-ethylenedioxythiophene):polystyrene sulfonate (PEDOT:PSS) material for redox function, which is suitable for real-time in vivo sensing of analytes. The electrode surface area was less important for the potentiometric sensing mechanism, suggesting the feasibility of using a tiny fiber-like electrode for potentiometric sensing. The output signal of the sensor was conditioned and processed using a small, portable, customized printed circuit board (PCB) and delivered to a terminal that included a computer or smartphone interface. Each microfilament sensing electrode (MSE) exhibited good sensitivity, linear range, and stability. In vivo tests in the subcutaneous space and cerebral cortex demonstrated that the continuous and real-time sensing of multiplex ions in complex environments was feasible. This study provides a versatile system for real-time monitoring of physiological ion fluctuations in multiple scenarios, with a huge potential to detect various biomarkers for comprehensive human health monitoring.

Materials and methods

Insulation of the Au microfilament electrode

Photocurable resin (Shenzhen Dayou Intelligent Printing Equipment Co., China) was used as an insulating material. The Au microfilament (about 100 μm in diameter) was inserted into a capillary glass tube (inner diameter of 200

μm and length of 30 mm) with 2 and 5 mm of the Au microfilament exposed at each end without insulation. The photocurable resin was injected into the capillary glass tube and irradiated with a 100% power ultraviolet (UV) lamp (Xiamen Lester Scientific Instruments Co., Ltd., China) for 60 s to cure it. The outer wall of the capillary glass tube was removed by rubbing to obtain a single Au microfilament insulated in the middle with both ends exposed.

Preparation of the polyvinyl butyral (PVB) coated Ag/AgCl microfilament electrode

Ag/AgCl ink (Yuncaitaotao Co., Ltd., Shenzhen, China) was coated onto the Au microfilament electrode (a section of 2 mm length). The Ag/AgCl-coated microfilament electrode was baked in an oven at 80 °C for 30 min to cure the Ag/AgCl ink. Finally, the Ag/AgCl microfilament electrode was immersed in 5% (mass fraction) PVB solution and dried at room temperature for 12 h to ensure that the PVB coating fully covered the Ag/AgCl material.

Preparation of the PEDOT:PSS-coated microfilament electrode

3,4-Ethylenedioxythiophene (EDOT) and poly(sodium 4-styrene sulfonate) (NaPSS) were obtained from Sigma-Aldrich corporation in Shanghai, China. EDOT:NaPSS aqueous solutions containing 0.01 mol/L EDOT and 0.1 mol/L NaPSS were prepared. An Au microfilament electrode (working electrode), a commercial Ag/AgCl reference electrode, and a Pt counter electrode were placed in this mixed solution. An electrochemical workstation was used to power the electrodes so that a constant current of 6 μA was applied to the Au microfilament electrode, which lasted for 700 s. PEDOT:PSS was modified into the Au microfilament electrode and used as an ion–electron converter to improve detection efficiency.

Preparation of K^+, Ca^{2+}, and Na^+ MSEs

Valinomycin (potassium ionophore), sodium tetraphenylborate (NaTPB), polyvinyl chloride (PVC), bis(2-ethylehexyl) sebacate (DOS), cyclohexanone, *N*,*N*,*N*',*N*'-Tetracyclohexyl-3-oxapentanediamide (ETH 129, calcium ionophore II), 1-nitro-2-(n-octyloxy)benzene (NPOE), tetrahydrofuran, Na ionophore III, and sodium tetrakis[3,5-bis(trifluoromethyl)phenyl] borate (Na-TFPB) were used to prepare ion-selective electrodes. All chemicals were obtained from Sigma-Aldrich in Shanghai, China. For the K^+-selective membrane, 200 mg of a cocktail comprising valinomycin (2%, mass fraction), NaTPB (0.53%, mass fraction), PVC (32.73%, mass fraction), and DOS (64.74%, mass fraction) was dissolved in 700 μL cyclohexanone. For the Ca^{2+}-selective membrane, 200 mg of a cocktail comprising ETH 129 (0.46%, mass fraction), NaTPB (0.48%, mass fraction), PVC (33.02%, mass fraction), and NPOE (66.04%, mass fraction) was dissolved in 1 mL tetrahydrofuran. For the Na^+-selective membrane, 200 mg of a cocktail comprising Na ionophore III (1%, mass fraction), Na-TFPB (0.55%, mass fraction), PVC (33%, mass fraction), and DOS (65.45%, mass fraction) was dissolved in 1320 μL tetrahydrofuran and shaken for 30 min. All ion-selective membrane coating solutions were sealed and stored at 4 °C when not used. The PEDOT:PSS-coated microfilament electrode was dip-coated with the K^+-selective membrane cocktail four times to obtain the K^+ MSE. The PEDOT:PSS-coated microfilament electrode was dip-coated with the Ca^{2+}-selective membrane cocktail four times to obtain the Ca^{2+} MSE. The PEDOT:PSS-coated microfilament electrode was dip-coated with the Na^+-selective membrane cocktail four times to obtain the Na^+ MSE. The electrodes were allowed to dry overnight in an ambient environment.

Assembly of MMEC

MMEC comprised a shared microfilament reference electrode (MRE) and K^+, Ca^{2+}, and Na^+ MSEs. The insulated segments of these four microfilament electrodes were tightly bonded in sequence using strong adhesive glue while exposing the tip of the MSE. When the four electrodes were integrated, they were modified as K^+, Ca^{2+}, and Na^+ sensing electrodes. An integrated modified MMEC was obtained.

Preparation of the Na^+ planar electrode

The Na^+ planar electrode consisted of a flexible PI as the substrate, a photocurable resin as the insulating layer, and Au as the conducting layer. A mask was placed on the PI substrate, and the Au layer was sputtered to obtain a patterned Au conductive layer. To avoid signal interference, the wiring section was covered with the photocurable resin to insulate it. An Au planar electrode with a sensing radius of 2 mm was obtained. For electrode modification, EDOT:NaPSS aqueous solutions containing 0.01 mol/L EDOT and 0.1 mol/L NaPSS were prepared. An Au planar electrode (working electrode), a commercial Ag/AgCl reference electrode, and a Pt counter electrode were placed in the EDOT:NaPSS mixed solution. An electrochemical workstation was used to power the electrodes so that a constant current of 14 μA was applied to the Au planar electrode, which lasted for 700 s. PEDOT:PSS was modified into the Au planar electrode and used as an ion–electron converter to improve detection efficiency. The PEDOT:PSS-coated planar electrode was dip-coated with the Na^+-selective membrane cocktail four times to obtain the Na^+ planar electrode. The electrodes were allowed to dry overnight in an ambient environment.

Preparation of the Na^+ spot electrode

The Au microfilament (about 100 μm in diameter) was insulated with a photocurable resin, and a section of the resin-coated Au wire was cut to expose the cross section of the Au wire (spot electrode) for sensing. Prepared EDOT:NaPSS aqueous solutions containing 0.01 mol/L EDOT and 0.1 mol/L NaPSS, an Au spot electrode (working electrode), a commercial Ag/AgCl reference electrode, and a Pt counter electrode were placed in this mixed solution. An electrochemical workstation was used to power the electrodes so that a constant current of 6 μA was applied to the Au spot electrode, which lasted for 700 s. PEDOT:PSS was modified into the Au spot electrode and used as an ion–electron converter to improve detection efficiency. The PEDOT:PSS-coated spot electrode was dip-coated with the Na^+-selective membrane cocktail four times to obtain the Na^+ spot electrode. The electrodes were allowed to dry overnight in an ambient environment.

In vitro characterization of MSE

The CHI 760E workstation (CH Instruments, Inc., USA), a commercial Ag/AgCl reference electrode, and MSE (including MRE) were used to conduct a series of characterizations to evaluate the performance of MSE. All solutions were prepared using deionized (DI) water (18.3 MΩ·cm) produced from a Millipore water purification system unless otherwise noted. The two-electrode system, with MSE as the working electrode and a commercial Ag/AgCl electrode as the reference electrode, was submerged in a solution for electrochemical sensing tests. The response curve of the MSE was obtained from a stairstep test using the ion concentration range in human blood as a reference. The K^+, Ca^{2+}, and Na^+ test ranges were 2–32, 0.5–4, and 10–160 mmol/L, respectively. During the test, the ion solution was replaced to change the ion concentration of the working electrode, the test was paused while the solution was being replaced, and the ion solution was left to stabilize for 60 s before continuing the test. For the ion selectivity test, multiple interfering substances and the corresponding markers were evaluated using sequential additions to the aqueous solution. For the K^+ selectivity test, 0.5 mmol/L $CaCl_2$, 2 mmol/L KCl, 10 mmol/L NaCl, 0.5 mmol/L $MgCl_2$, and 0.5 mmol/L $CaCl_2$ were added to DI water. For the Ca^{2+} selectivity test, 0.5 mmol/L $MgCl_2$, 0.5 mmol/L $CaCl_2$, 10 mmol/L NaCl, 2 mmol/L KCl, and 0.5 mmol/L $MgCl_2$ were added to DI water. For the Na^+ selectivity test, 0.5 mmol/L $CaCl_2$, 10 mmol/L NaCl, 2 mmol/L KCl, 0.5 mmol/L $MgCl_2$, and 0.5 mmol/L $CaCl_2$ were added to DI water.

Fabrication and use of PCB

Altium Designer was used to design the circuit structure of the system and the layout wiring of PCB to complete the design of the entire circuit. PCB was populated with components, the program was burned, an external battery was used as a power supply, and the sensor was connected to realize the complete system to support the signal acquisition, processing, display, and storage functions of the sensor device. The ion sensor obtained the potential corresponding to ion concentrations from the detection environment, and the signal was amplified using a signal amplifier before input to microcontroller unit (MCU) for analog-to-digital conversion and digital signal processing. Finally, the processed result was sent to an Android-based mobile application for data display and storage by wireless transmission to monitor ion concentration changes in real time.

In vivo experiments

Female Sprague–Dawley (SD) rats weighing 220–250 g, about eight weeks old (Sun Yat-Sen University Animal Center, Guangzhou, China), were used for the experiments. All rats were raised in a barrier environment, with 2% pentobarbital sodium injected intraperitoneally in the laboratory at 0.3 mL/100 g body weight.

Subcutaneous monitoring of multiple ions in living rats

The integrated MMEC was used as a sensor for subcutaneous ion detection in living rats. The PVB-coated Ag/AgCl microfilament electrode of MMEC was used as a shared reference electrode, whereas K^+, Ca^{2+}, and Na^+ MSEs of MMEC were used as working electrodes. First, 2% pentobarbital sodium was injected intraperitoneally into SD rats. After successful anesthesia, the hair on the back of the rat was shaved. A syringe with an outer diameter of 1.2 mm was used to poke the skin on the back. An about 1 mm MMEC was inserted into the epidermis of the rat and fixed. The electrochemical workstation collected potentiometric signals from the two-electrode system, and results were recorded every 15 min for 3 h. At each recording time point, the recording of the potentiometric signal lasted for 1 min to allow signal stabilization. Blood from rat tails was collected before and after the test, and the plasma was centrifuged immediately after collection. Finally, the ion concentration in the serum was measured using an automatic dielectric analyzer (HC-9885; Shenzhen Hangchuang Medical Equipment Co., China) as reference ion concentration.

In vivo multiple ion monitoring in the rat cerebral cortex

The integrated MMEC was used as a sensor for ion detection in the cerebral cortex of living rats. First, SD rats were injected intraperitoneally with 2% pentobarbital sodium. After the rats were successfully anesthetized, hair from the scalp was shaved, and the rats were fixed. The scalp was gently removed using scalpels and forceps, and the skull was opened with a cranial drill with a diameter of 2 mm. Immediately afterward, the meninges above the cerebral cortex were removed using scalpels and forceps to expose the cerebral cortex with a diameter of 2 mm. MMEC was placed into the cerebral cortex through the openings and fixed using a fixation table. Potentiometric signals were collected by the two-electrode system using an electrochemical workstation, and results were recorded every 15 min for 3 h.

Analysis of ion concentrations in tissue

Using the reference value of serum ions obtained before and after the subcutaneous test, subcutaneous data measured by the MSE cluster were calibrated using the two-point method (y=kx+b), which was applied to the brain test results to obtain ion values in the brain. Herein, y denotes the current value measured by MMEC, x denotes the ion concentration (K^+, Ca^{2+}, and Na^+), k is the slope of the calibration curve (indicating the sensitivity of the electrode), and b denotes the intercept of the calibration curve.

Results and discussion

Figure 1d shows the semi-implantable multiplexed ion-sensing system comprising an MMEC device, a multichannel customized PCB for ion concentration detection, and display terminals. The MMEC device comprised a shared MRE and three ion-selective working electrodes based on Au microfilament, including K^+, Ca^{2+}, and Na^+ MSEs. Working and reference electrodes can be employed for potentiometric sensing and determining target ion concentrations in various biological environments. The three microfilament ion-selective working electrodes of the MMEC utilized the shared MRE for sensing. The sensing of different ions was alternately performed to prevent interference with each other when using the shared reference electrode. PCB for ion concentration detection was constructed to support the operation of MMEC, allowing it to be a miniature and portable system for a wide range of sensing scenarios on living bodies. Through an integrated design, the size of the portable PCB for ion concentration detection was smaller than 4.5 cm × 5.0 cm. Display terminals included computer and mobile smartphone terminals that could be freely incorporated based on experimental needs. The computer terminal and the universal serial bus (USB) interface on the PCB for ion concentration detection were used in conjunction, whereas the mobile smartphone terminal and Bluetooth on the PCB for ion concentration detection were used in conjunction.

The fabrication process of the MMEC device for three types of ion sensing is shown in Fig. 2a. In short, clean Au microfilaments with a diameter of 0.1 mm possessing good biocompatibility and electrical properties were insulated using a photocurable resin. For the reference electrode, one tip of the insulated microfilament electrode was dipped in an Ag/AgCl and PVB solution, and the PVB-coated Ag/AgCl microfilament electrode was used as MRE. For the working electrodes, PEDOT:PSS was first electroplated as a redox layer on the top of the insulated microfilament electrodes, named the PEDOT:PSS-coated microfilament electrode. Three types of ion-selective membrane solutions were applied on the surface of the PEDOT:PSS-coated microfilament electrodes and dried at room temperature overnight to obtain three MSEs. Finally, an MRE and three MSEs were integrated to obtain the MMEC device.

In Fig. 2b, each MSE in the completed MMEC device was connected to the same MRE to form a two-electrode system to detect sample ion concentrations. The flexible and miniature feature of the MMEC device could potentially have good biocompatibility with tissues and reduce microfilament tissue damage after implantation (Fig. S1 in Supplementary Information). Figures 2c, 2d and Fig. S2 (Supplementary Information) show the working principle of MSE and the PVB-coated Ag/AgCl microfilament electrode in this work. In Fig. 2c, PEDOT:PSS conducting polymers were used as functional materials for electrodeposition on Au substrates of MSE to convert charge carriers from ions to electrons. This redox reaction can be expressed as follows:

$$\mathrm{PEDOT^+PSS^-} + I^+ + e^- \rightleftharpoons \mathrm{PEDOT^\circ PSS^-}I^+, \tag{1a}$$

$$\mathrm{PEDOT^+}R^- + e^- \rightleftharpoons \mathrm{PEDOT^\circ} + R^-, \tag{1b}$$

where $PEDOT^+$ is an oxidized conductive polymer unit, PSS^- is an anion doped in PEDOT, e^- is the mobile electron, and PEDOT° is a neutral conductive polymer unit. I^+ and R^- denote the primary cation (e.g., K^+, Ca^{2+}, and Na^+) and lipophilic anionic site (e.g., tetraphenylborate derivatives) respectively, which could cross the interface between the MSE membrane and the conducting polymer membrane. The contribution of the reactions expressed by Eqs. (1a) and (1b) was related to the number of I^+ and R^- transfers and their mobility. This allowed the quantification of the ions in the reaction. For conducting polymers doped with large volumes of immobile PSS^- polyelectrolytes, the ion exchange at the MSE film/conductive polymer interface was dominated

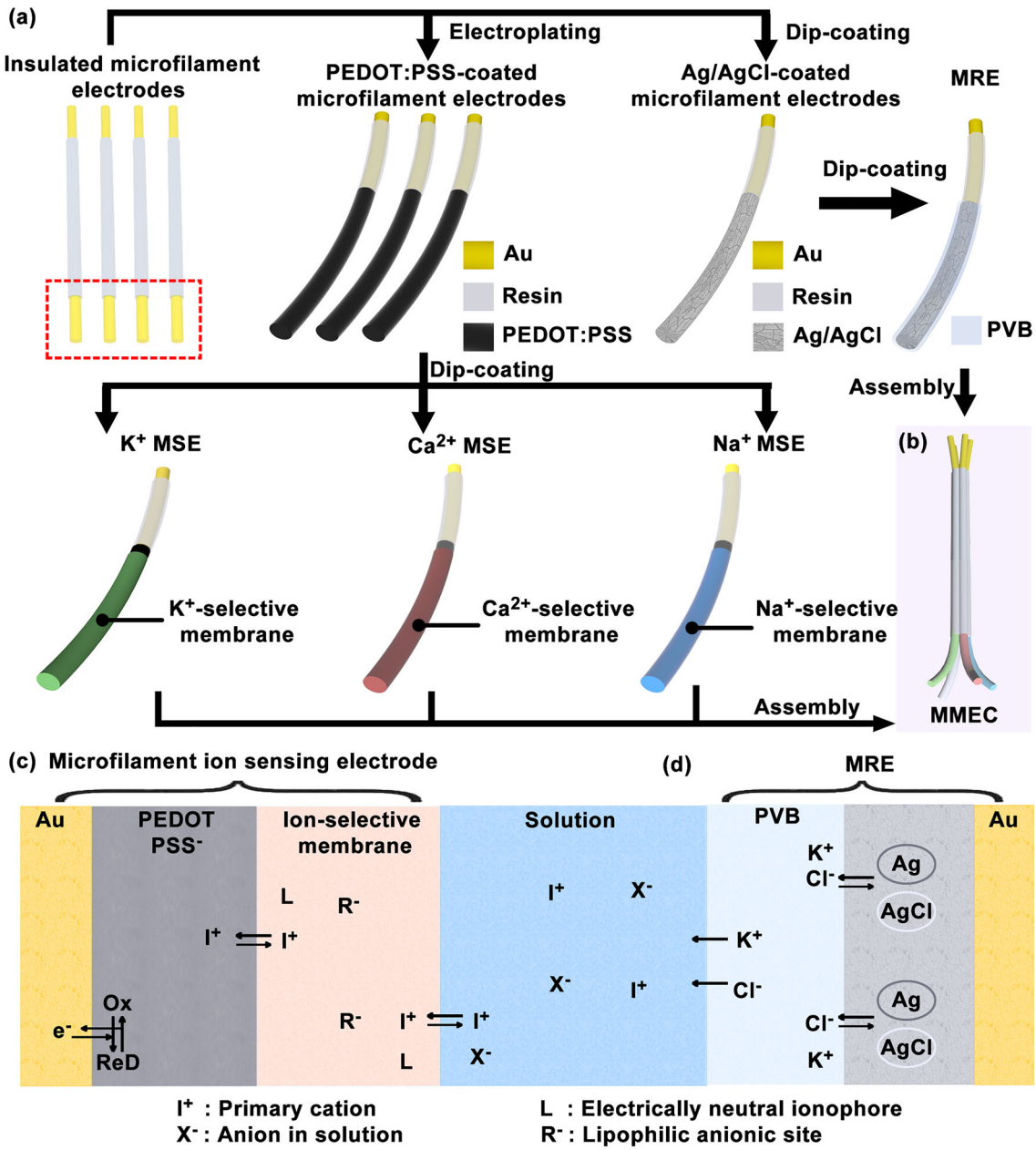

Fig. 2 Schematic diagram of the preparation process and working principle of MMEC. **a** Preparation process of ion-sensing electrodes. First, Au microfilament electrodes were insulated with photocurable resins. The tips of the insulated microfilament electrodes were electroplated with the PEDOT:PSS solution and dip-coated with Ag/AgCl slurry. The working electrodes were modified by dip-coating the PEDOT:PSS-coated electrodes with K^+-, Ca^{2+}-, and Na^+-selective membranes. For the reference electrode, the Ag/AgCl electrode was dip-coated with a PVB film. **b** Schematic diagram of the completed Au MMEC for three ion-sensing devices after multilayer modification. The MMEC ion sensor contains one shared reference electrode and three working electrodes. The three working electrodes include microfilament electrodes for Na^+, K^+, and Ca^{2+} sensing, respectively. **c** Working principle of ion-selective electrodes of MMEC (Ox: oxidation reaction; ReD: reduction reaction). **d** Working principle of MRE of MMEC. MMEC: multiplexed microfilament electrode cluster; PEDOT:PSS: poly(3,4-ethylenedioxythiophene):polystyrene sulfonate; PVB: polyvinyl butyral; MRE: microfilament reference electrode; MSE: microfilament sensing electrode

by I^+ cations in Eq. (1a), with Eq. (1b) being complementary. Thus, the redox reactions expressed by Eqs. (1a) and (1b) in the conducting polymer layer control the interfacial potential between the conducting polymer and the electron-conducting substrate, whereas the potential difference across the interface of the MSE film and the conducting polymer was determined by the ion distribution between these two phases.

Moreover, the ion concentration in the sample to be measured could influence the level of each interfacial potential, from which the ion concentration in the sample solution is inferred. In Fig. 2d, the MRE comprised a hydrophilic polymer (PVB) layer on its surface containing a saturated KCl electrolyte wrapping around the Ag/AgCl mixture. Similar to the conventional Ag/AgCl electrode, the Ag/AgCl layer of MRE and the internally filled solution containing constant active primary ions and Cl^- led to a reversible redox reaction [$AgCl(s) + e^- \rightleftharpoons Ag(s) + Cl^-$ (aq)] to achieve a balance of charge conduction from ions to electrons. The PVB-coated Ag/AgCl microfilament electrode showed good long-term stability compared to the conventional Ag/AgCl reference electrode due to the ability of the PVB layer to maintain a constant Cl^- concentration within the membrane.

The surface morphology of MMEC devices was characterized during preparation using optical microscopy and scanning electron microscopy (SEM). Figure 3a shows the initial Au microfilament with a diameter of about 100 μm (purity >99.99%) without modification. The total diameter of the Au microfilament electrode insulated by the photocurable resin was about 200 μm, while the exposed tip length was about 2 mm (Fig. 3b and Figs. S3 and S4 in Supplementary Information). The SEM image of the Au microfilament electrode is shown in Fig. 3c. The SEM image of the PVB-coated Ag/AgCl microfilament electrode is shown in Fig. 3d, which was used as MRE in the MMEC. The thickness of the coating PEDOT:PSS material was about 1–3 μm, whereas the thickness of the coated Ag/AgCl material was about 5–10 μm (Fig. S5 in Supplementary Information). Figure 3e shows the detailed SEM images of the PEDOT:PSS-coated microfilament electrode; the left image was under low magnification, and the right image was under high magnification. In the figure, the surface of the Au microfilament electrode after PEDOT:PSS modification was smooth and uniform. Figures 3f–3h present the detailed SEM images of K^+, Ca^{2+}, and Na^+ MSEs respectively, showing that K^+, Ca^{2+}, and Na^+ MSEs still exhibited flat surface morphology. Finally, Fig. 3i shows the completed modified integrated MMEC device, which formed the three-part set of the two-electrode sensing system to measure K^+, Ca^{2+}, and Na^+ ion concentrations in a 2 mm × 2 mm region (Fig. S6 in Supplementary Information). The electrodes could be affixed/implanted at many different tissue sites because the functional area of the device occupied a small volume and remained flexible when coated with different coatings. Different microfilament electrodes were integrated side-by-side, forming a flexible semi-implantable MMEC device using polydimethylsiloxane packaging.

Because the surface area of the semi-implantable microfilament electrode was generally smaller than that of conventional planar electrodes, the sensing performance of this tiny fiber-like electrode was likely to be limited due to its size (about 0.322 mm^2). This study investigated the sensing characteristics of the microfilament electrodes and compared them to electrodes with different surface areas. The planar electrode (electrode radius: 2 mm) was prepared by sputtering an Au conducting layer on a flexible PI substrate, where electric leads were insulated by resins (Fig. 4a). The microfilament electrode consisted of an Au wire with a 50 μm radius covered with photocurable resins, and the electrode exposed a tip with a length of 1 mm as the sensing area (Fig. 4b). The spot-like electrode was composed of an Au wire with a 50 μm radius covered with photocurable resins on all sidewalls, and the spot electrode only exposed a dot on the end of the electrode as the sensing area (Fig. 4c). The sensing performance (including linear relationship sensitivity), electrode variation, and linear correlation coefficient (R^2) of these electrodes with different sensing areas were evaluated and compared. The area of the studied electrodes is summarized in Fig. 4d, where the microfilament electrode area was 0.322 mm^2, the planar electrode area was 12.566 mm^2 (about 40 times that of the microfilament electrode), and the spot electrode area was 0.008 mm^2 (about 1/40 that of the microfilament electrode). For electrode modification, all three electrodes were electroplated with PEDOT:PSS as the electron mediator, and the outermost layer was coated with a Na^+-selective film. Next, the three ion electrodes were placed in a Na^+ aqueous solution for a potentiometric sensing test. Based on the Na^+ concentration range in the human body between 136 and 150 mmol/L [28, 38], tests were performed using NaCl solutions at concentrations of 10–160 mmol/L. Figure 4e shows the potentiometric signal measured by three Na^+ planar electrodes in different concentrations of NaCl solution and the linear relationship between this potential signal and the logarithm of Na^+ concentration. Similarly, Figs. 4f and 4g show the detection performances of Na^+ MSEs and Na^+ spot electrodes for Na^+ ions, respectively.

Furthermore, the sensitivity (slope of the fitting curve), electrode variation, and R^2 of the three electrodes were statistically analyzed (Fig. S7 in Supplementary Information). The microfilament electrode exhibited good sensing sensitivity with a small sensing area and good linear fit, indicating that the microfilament electrode was a good candidate for a semi-implantable ion-sensing electrode. To test the long-term stability of Na^+ MSE, its sensitivity was detected on Days 1, 3, 7, and 14, and the results indicated that the sensor sensitivity remained stable (changed by <20%) for at least 14 days after the preparation (Fig. 4h).

Moreover, to validate the adhesion stability of the device's surface materials, a sample of the Na^+ ion-selective membrane (Na^+ MSE) was taken, and the electrode was subjected to immersion in a stirred solution or exposure to in vitro tissues for 12 h, followed by observing changes in its surface structure. Compared to the untreated Na^+ MSE control group (Fig. 4i), the overall material structure on the surface of the Na^+ MSE that had been immersed in solution or implanted

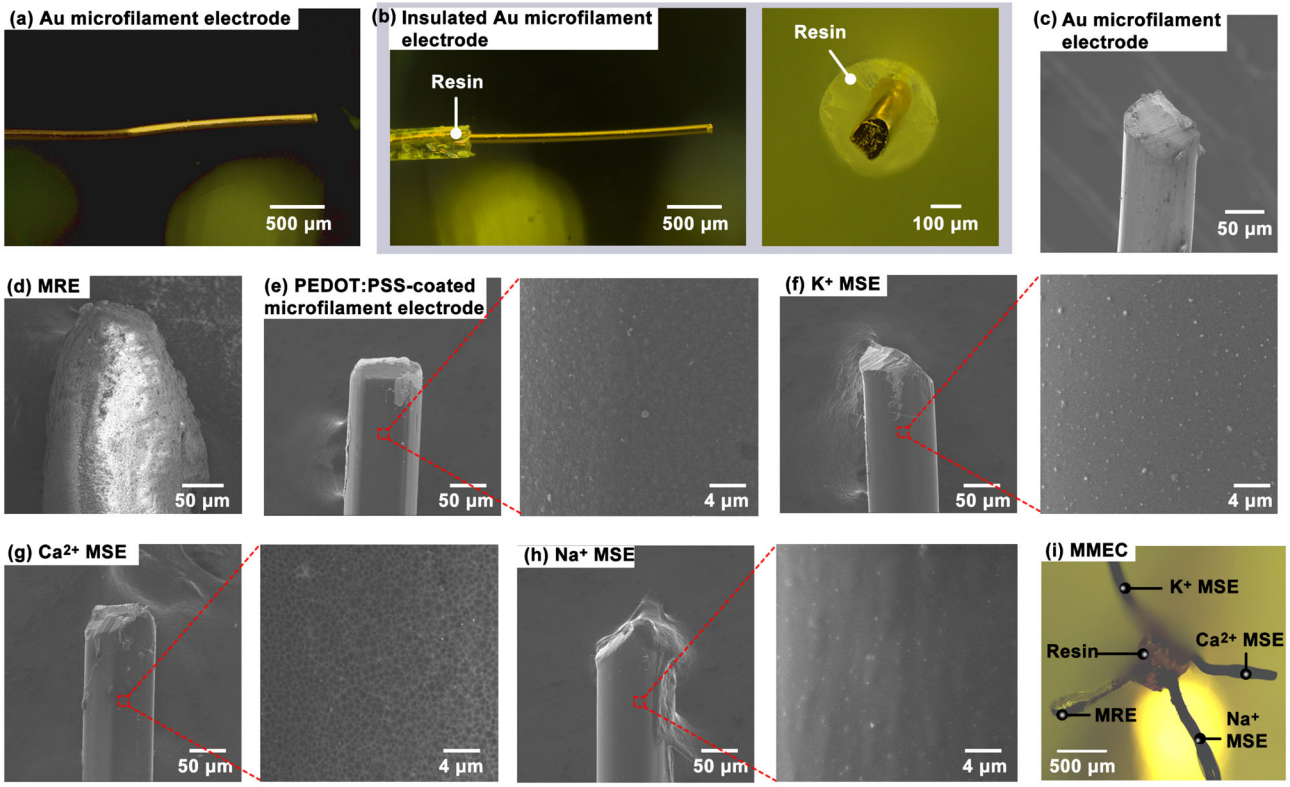

Fig. 3 Morphological structure of MMEC. **a** Optical micrograph of the Au microfilament electrode. **b** Optical micrograph of an insulated Au microfilament electrode with an insulating layer: side view (left) and cross-sectional view (right). **c** SEM image of the insulated Au microfilament electrode. **d** SEM image of MRE in MMEC. **e** SEM image of the PEDOT:PSS-coated microfilament electrode under low magnification (left) and high magnification (right). **f** SEM image of the completed modified K^+ MSE. **g** SEM image of the completed modified Ca^{2+} MSE. **h** SEM image of the completed modified Na^+ MSE. **i** Optical micrograph of MMEC with triple ion-sensing function assembled from MRE and K^+, Ca^{2+}, and Na^+ MSEs. MMEC: multiplexed microfilament electrode cluster; SEM: scanning electron microscopy; MRE: microfilament reference electrode; PEDOT:PSS: poly(3,4-ethylenedioxythiophene):polystyrene sulfonate; MSE: microfilament sensing electrode

in excised tissue remained intact. Moreover, the material in localized regions continued to uniformly cover the electrode surface (Figs. 4j and 4k). SEM results showed that the functional material of the microfilament ion electrode can stably adhere to the electrode surface, ensuring the stability of the electrode performance.

Because the semi-implantable MMEC device could sense Na^+, K^+, and Ca^{2+} simultaneously, the sensing performance of each microfilament electrode in the device was verified by in vitro experiments. The MMEC device contained Na^+, K^+, and Ca^{2+} MSEs and a shared PVB-coated Ag/AgCl MRE. The shared MRE allowed the integrated three-parameter sensor device to contain only one MRE, reducing the device's size compared to conventional three-reference-electrode devices. Also, the PVB-coated Ag/AgCl microfilament electrode had better stability and a lower baseline than the conventional Ag/AgCl electrode. For wearable devices, smaller testing volumes and stable electrical signals are vital for safety and prolonged sensing in biological environments.

For in vitro ion sensing, a two-electrode system comprising Na^+, K^+, or Ca^{2+} MSEs and a reference electrode (Fig. 5a) was validated separately. The step signals for in vitro experiments in Fig. 5 were tested by replacing the samples with different concentrations. To avoid introducing additional noise interference, data recording was paused for 60 s when changing samples. The data sampling rate for all open-circuit potential signals was 10 Hz. Figure 5b shows that the PVB-coated Ag/AgCl microfilament electrode not only possessed good stability (Fig. S8 in Supplementary Information) but also exhibited a low signal background in DI water or different concentrations of Cl^- salt solutions. Therefore, choosing a PVB-coated Ag/AgCl microfilament electrode as a reference electrode for MMEC devices was more accurate and stable than an Ag/AgCl microfilament electrode.

Because the K^+ concentration in the human body ranges from 2.7 to 5.5 mmol/L [28, 42], K^+ was tested in KCl

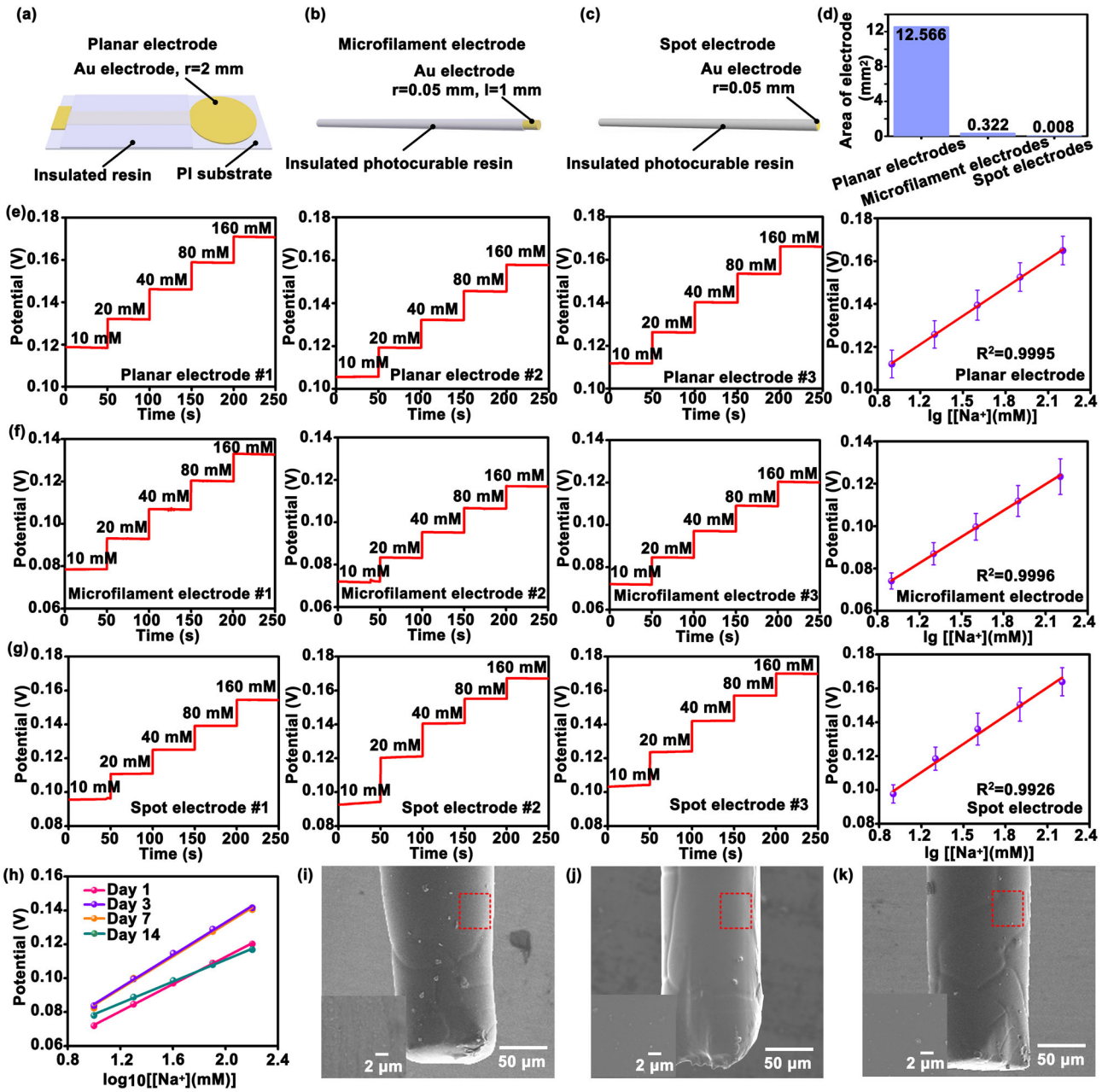

Fig. 4 Comparison of the Na^+ sensing performance of planar, microfilament, and spot electrodes. Schematic diagram of the **a** planar, **b** microfilament, and **c** spot electrodes. **d** Comparison of the area of the planar, microfilament, and spot electrodes. **e** Potentiometric signals were measured by three Na^+ planar electrodes in different concentrations of NaCl solution, and the linear relationship curve was between the potentiometric signal and the logarithm of Na^+ concentration. **f** Potentiometric signals were measured by three Na^+ MSEs in different concentrations of NaCl solution, and the linear relationship curve was between the potentiometric signal and the logarithm of Na^+ concentration. **g** Potentiometric signals were measured by three Na^+ spot electrodes in different concentrations of NaCl solution, and the linear relationship curve was between the potentiometric signal and the logarithm of Na^+ concentration. **h** Sensing performance of Na^+ MSE on Days 1, 3, 7, and 14. **i** SEM images of untreated Na^+ MSE. **j** SEM images of Na^+ MSE after 12 h of immersion in a stirred solution. **k** SEM images of Na^+ MSE at 12 h after implantation in excised tissue. For the fourth column of (e)–(g), data are represented as mean±standard deviation (n=3). MSE: microfilament sensing electrode; SEM: scanning electron microscopy; PI: polyimide; mM: mmol/L

solutions of 2–32 mmol/L (Fig. 5c). In Fig. 5c1, the potentiometric signal of KCl aqueous solutions with different concentrations was detected by K^+ MSE of the MMEC device by changing the solution every 50 s. There was a clear linear relationship between the potentiometric signal and the logarithm of K^+ concentration as the KCl solution concentration increased from 2 to 32 mmol/L (Fig. 5c2). The slope of the linear relationship was 36.7 mV/decade,

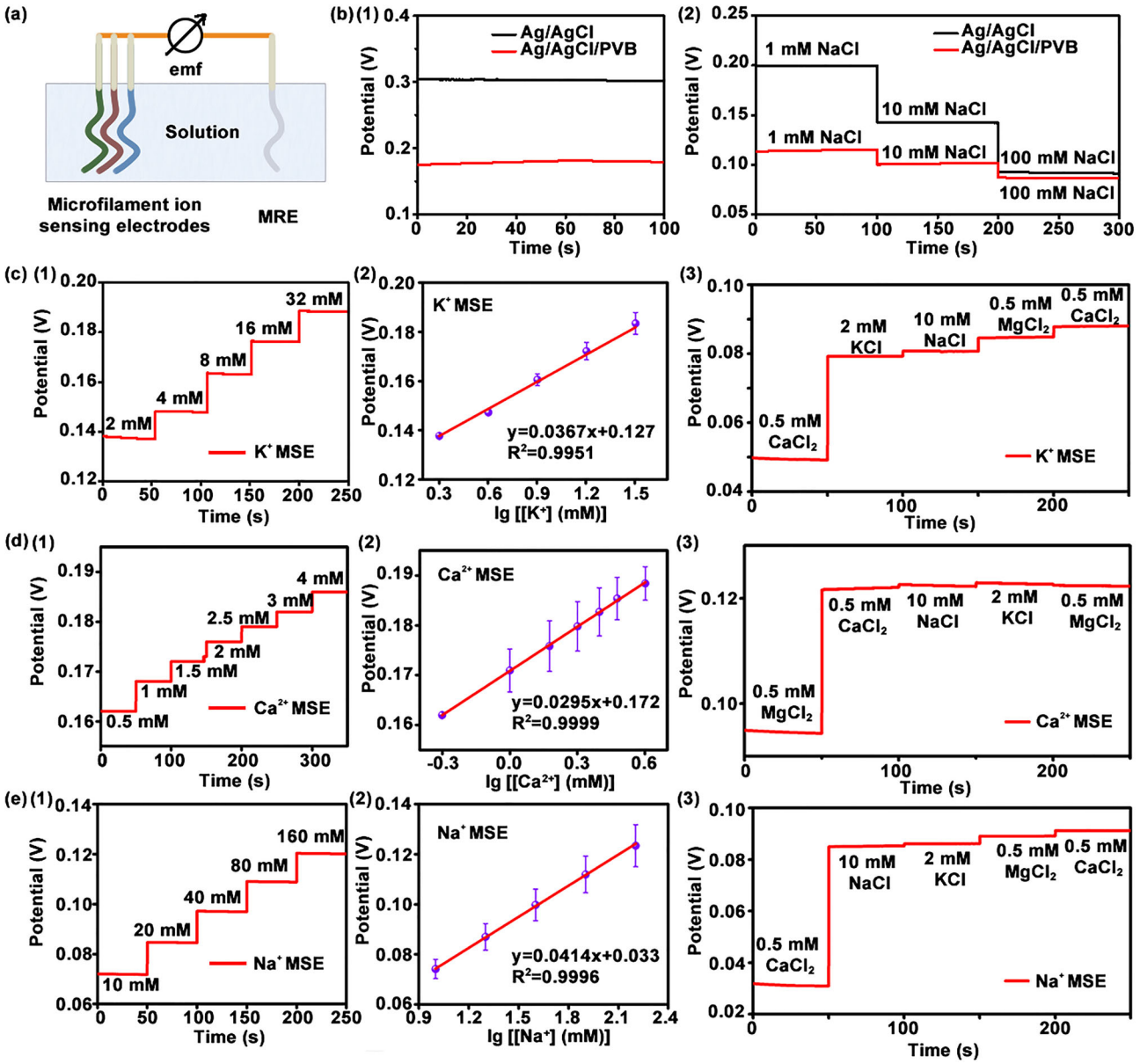

Fig. 5 Performance of MSE for detection of K^+, Ca^{2+}, and Na^+ concentrations. **a** Schematic diagram of the two-electrode potentiometric signal detection system. **b** Potentiometric signals of the homemade microfilament Ag/AgCl electrode and microfilament Ag/AgCl/PVB electrode as working electrodes in (1) DI water and (2) 1, 10, and 100 mmol/L NaCl solutions when the reference electrode was a commercial Ag/AgCl electrode. **c** Potentiometric signal detection performance of K^+ MSE: (1) potential response of K^+ MSE in 2, 4, 8, 16, and 32 mmol/L K^+ solutions; (2) concentration–potential curve of K^+ MSE in 2–32 mmol/L K^+ solutions; (3) evaluation of anti-interference performance of K^+ sensors. Here, 0.5 mmol/L $CaCl_2$, 2 mmol/L KCl, 10 mmol/L NaCl, 0.5 mmol/L $MgCl_2$, and 0.5 mmol/L $CaCl_2$ were added to the aqueous solution in sequence. **d** Potentiometric signal detection performance of Ca^{2+} MSE: (1) potential response of Ca^{2+} sensor in 0.5, 1, 1.5, 2, 2.5, 3, and 4 mmol/L Ca^{2+} solutions; (2) concentration–potential curve of Ca^{2+} MSE in 0.5–4 mmol/L Ca^{2+} solutions; (3) evaluation of anti-interference performance of Ca^{2+} sensors. Here, 0.5 mmol/L $MgCl_2$, 0.5 mmol/L $CaCl_2$, 10 mmol/L NaCl, 2 mmol/L KCl, and 0.5 mmol/L $MgCl_2$ were added to the aqueous solution in sequence. **e** Potentiometric signal detection performance of Na^+ MSE: (1) potential response of Na^+ sensor in 10, 20, 40, 80, and 160 mmol/L K^+ solutions; (2) concentration–potential curve of Na^+ MSE in 10–160 mmol/L Na^+ solutions; (3) interference immunity assessment of Na^+ sensors. Here, 0.5 mmol/L $CaCl_2$, 10 mmol/L NaCl, 2 mmol/L KCl, 0.5 mmol/L $MgCl_2$, and 0.5 mmol/L $CaCl_2$ were added to the aqueous solution in sequence. Data recording was suspended for 60 s when the solutions were changed. For the second column of (c)–(e), data are represented as mean±standard deviation (n=3). MSE: microfilament sensing electrode; MRE: microfilament reference electrode; PVB: polyvinyl butyral; DI: deionized; mM: mmol/L

and the R^2 for K^+ was 0.995, indicating the potential of K^+ MSE to quantitatively detect K^+ in solution. Figure 5c3 shows the potentiometric signal measured by K^+ MSE when 0.5 mmol/L $CaCl_2$, 2 mmol/L KCl, 10 mmol/L NaCl, 0.5

mmol/L $MgCl_2$, and 0.5 mmol/L $CaCl_2$ were added to DI water. In anti-interference experiments, different ion concentrations were determined based on ion concentration ratios within the body [43]. K^+ MSE showed the most obvious potentiometric signal for KCl, indicating that the K^+ microfilament electrode could selectively detect K^+ while avoiding the interference of other ions.

Since the Ca^{2+} concentration in the human body is between 1 and 2.75 mmol/L [28, 42], Ca^{2+} was tested in $CaCl_2$ aqueous solutions of 0.5–4 mmol/L (Fig. 5d). The potentiometric signal of the $CaCl_2$ aqueous solution with a concentration gradient was detected by Ca^{2+} MSE of the MMEC device, and the solution was changed every 50 s to obtain the step signal shown in Fig. 5d1. A linear relationship with a slope of 29.5 mV/decade and an R^2 of 0.9999 was acquired between the potentiometric signal and the logarithm of Ca^{2+} concentration as the $CaCl_2$ solution concentration increased from 0.5 to 4 mmol/L (Fig. 5d2). Figure 5d3 shows potentiometric signals measured by Ca^{2+} MSE when 0.5 mmol/L $MgCl_2$, 0.5 mmol/L $CaCl_2$, 10 mmol/L NaCl, 2 mmol/L KCl, and 0.5 mmol/L $MgCl_2$ were added to DI water. Ca^{2+} MSE showed the most obvious potentiometric signal for $CaCl_2$, indicating that the Ca^{2+} microfilament electrode could selectively detect Ca^{2+} while avoiding the interference of other ions (Fig. S9 in Supplementary Information).

Like K^+ and Ca^{2+} MSEs, Na^+ MSE of the MMEC device was tested in different concentrations (10–160 mmol/L) of NaCl aqueous solutions. The potentiometric signal of Na^+ MSE detecting NaCl aqueous solutions with different concentration gradients is shown in Fig. 5e1. A linear relationship between this potentiometric signal and the logarithm of Na^+ concentration was obtained with a slope of 41.4 mV/decade and an R^2 of 0.9996, as shown in Fig. 5e2. Figure 5e3 shows the potentiometric signal measured by Na^+ MSE when 0.5 mmol/L $CaCl_2$, 10 mmol/L NaCl, 2 mmol/L KCl, 0.5 mmol/L $MgCl_2$, and 0.5 mmol/L $CaCl_2$ were added to DI water. The maximum response of Na^+ MSE to the potentiometric signal of Na^+ indicated that the Na^+ microfilament electrode could selectively detect Na^+ while avoiding the interference of other ions. In summary, in vitro solution experiments verified the good detection performance of MRE and K^+, Ca^{2+}, and Na^+ MSEs in MMEC devices.

To evaluate the monitoring performance of MMEC in ISF in vivo, MMEC was implanted subcutaneously for in situ and continuous recording of physiological ion concentrations. The dorsal skin hair of rats was shaved, and rats were anesthetized and fixed for experimental tests. The dorsal skin was poked with a needle, and the flexible MMEC was implanted into the poked tissue. In vivo K^+, Ca^{2+}, and Na^+ concentrations were recorded with MMEC by measuring potentiometric signals every 15 min. At each recording time point, the recording of the potentiometric signal lasted 1 min to allow signal stabilization. To avoid signal crosstalk among different ions, the recording of different ions was performed separately using the shared MRE. The alternate use of shared electrodes and separated recording were allowed because the ion concentration fluctuation in vivo was generally at a slow frequency. The recording lasted for 3 h because prolonged anesthesia of rats would compromise their health. Na^+, K^+, and Ca^{2+} concentrations in rat blood were highly correlated with ion concentrations in the tissue fluid. Blood from rat tails was collected at the beginning and end of the in vivo recording experiment, and blood K^+, Ca^{2+}, and Na^+ concentrations were measured using a commercially available automatic dielectric analyzer. To convert the measured potentiometric signals into ion concentrations, a standard curve of the ion concentration versus the potentiometric signal was established using a two-point correction method by correlating the measured ion concentrations in the blood to corresponding potentiometric signal intensities. With the established standard curve, the corresponding ion concentration from the potentiometric signal measured by MMEC in ISF was calculated.

Figures 6a–6c show the in vivo subcutaneous monitoring results of each ion concentration (postcalibration) in anesthetized rats. The red dots in the figures represent the reference K^+, Ca^{2+}, and Na^+ concentrations in the serum at specific time points, as measured using an automated potentiometric analyzer. The concentration of each of the three types of ions was measured every 15 min, and each measurement was maintained for 1 min to stabilize the signals. The inset plots show the 1 min signal stabilization curves for MMEC sensing of K^+, Ca^{2+}, and Na^+ at a specific time point. During the three-hour testing period, K^+ concentration gradually increased from 4.29 to 4.31 mmol/L, Ca^{2+} concentration increased from 1.24 to 1.25 mmol/L, and Na^+ concentration fluctuated from 142 to 147 mmol/L. Resulting fluctuations in MMEC-measured ion concentrations were likely due to corresponding fluctuations in ion metabolism in the rat during anesthesia. Alternatively, the measured ion concentrations might also increase or fluctuate gradually due to the diffusion of subcutaneous ions into the electrode surface area after MMEC was inserted subcutaneously. The small fluctuations in the overall ion concentration were within the normal range. The average MMEC-measured K^+, Ca^{2+}, and Na^+ concentrations during the three-hour recording period were analyzed, as shown in Fig. 6d. This experiment also verified the potential use of this MMEC device in subcutaneous detection applications.

Continuous measurement of K^+, Ca^{2+}, and Na^+ in the living brain provided a more comprehensive understanding of physiological and pathological processes throughout the brain, as changes in electrical signals in the brain highly depend on chemical signals, such as neurotransmitters, or physiological ions. The feasibility of implanting MMEC in the brain to detect K^+, Ca^{2+}, and Na^+ concentrations was

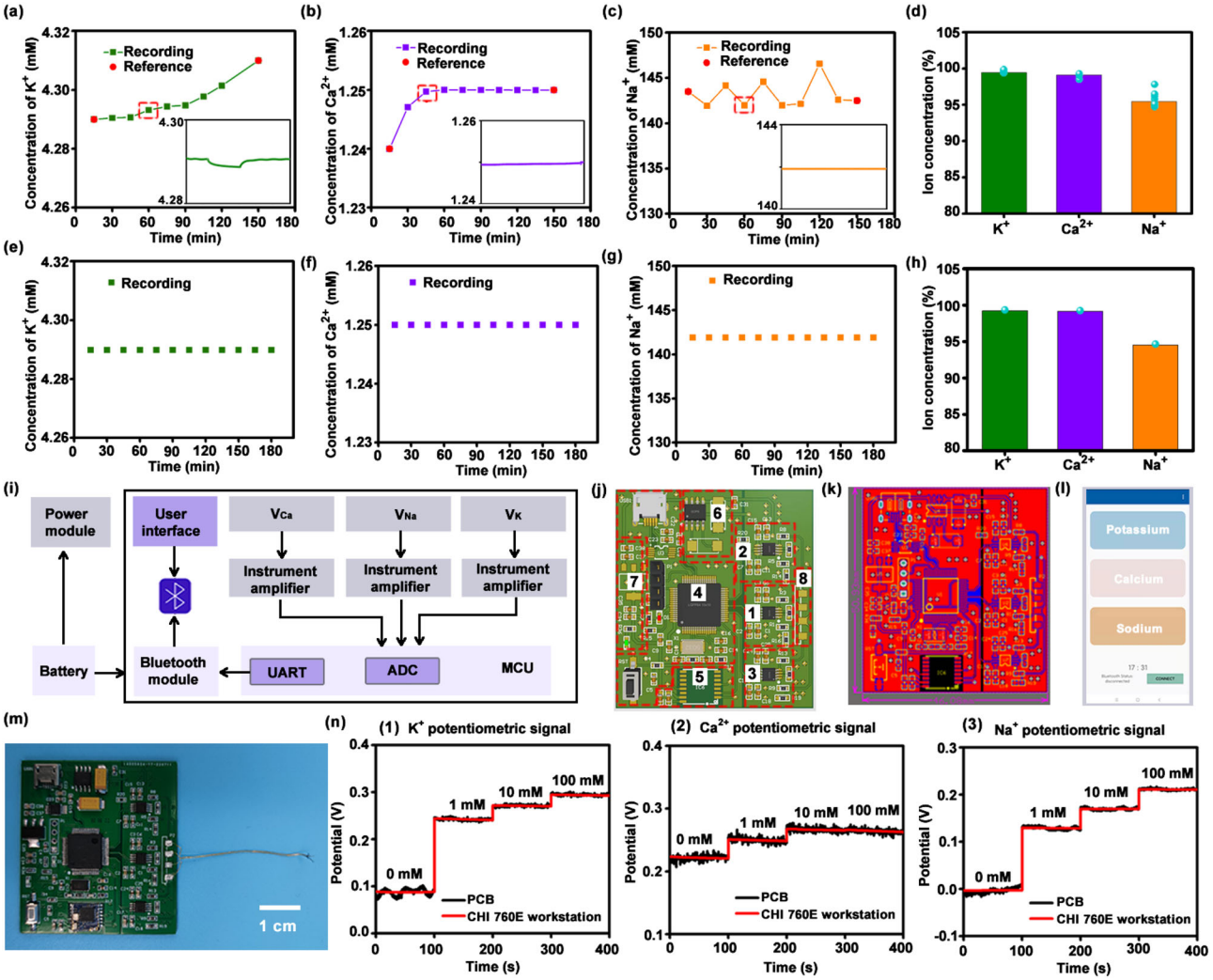

Fig. 6 In vivo continuous ion monitoring in rats using MMEC. **a** K^+ concentrations were detected using MMEC when the sensor was buried subcutaneously on the rat's back. Red dots in the plot represent the reference K^+ concentrations in the serum. The inset plot shows the 1 min signal stabilization curve for MMEC sensing of K^+ at the fourth data point. **b** Ca^{2+} concentrations were detected using MMEC when the sensor was buried subcutaneously on the rat's back. Red dots in the plot represent the reference Ca^{2+} concentrations in the serum. The inset plot shows the 1 min signal stabilization curve for MMEC sensing of Ca^{2+} at the third data point. **c** Na^+ concentrations were detected using MMEC when the sensor was buried subcutaneously on the rat's back. Red dots in the plot represent the reference Na^+ concentrations in the serum. The inset plot shows the 1 min signal stabilization curve for MMEC sensing of Na^+ at the fourth data point. **d** MMEC-measured average K^+, Ca^{2+}, and Na^+ concentrations during the 3 h recording period. The 100% value of K^+, Ca^{2+}, and Na^+ concentration was set as 4.32, 1.26, and 150 mmol/L, respectively. **e** K^+, **f** Ca^{2+}, and **g** Na^+ concentrations detected using MMEC when the sensor was buried in the cerebral cortex. **h** MMEC-measured average K^+, Ca^{2+}, and Na^+ concentrations in the brain during the 3 h recording period. The 100% value of K^+, Ca^{2+}, and Na^+ concentration was set as 4.32, 1.26, and 150 mmol/L, respectively. **i** Logic schematics of the MMEC system. **j** Eight functional modules of the customized PCB. **k** PCB diagram drawn by Altium Designer. **l** Mobile terminal software interface of the MMEC-based semi-implantable device system. **m** Integrated MMEC and customized PCB of the MMEC-based semi-implantable device system. **n** Comparison of potentiometric signals collected by MMEC-based semi-implantable device system and MMEC-based electrochemical workstation in the detection of (1) K^+, (2) Ca^{2+}, and (3) Na^+ in the in vitro solution. MMEC: multiplexed microfilament electrode cluster; PCB: printed circuit board; mM: mmol/L; UART: Universal Asynchronous Receiver/Transmitter; ADC: analog-to-digital converter; MCU: microcontroller unit

evaluated. The scalp hair of rats was shaved, and rats were anesthetized and fixed. Next, surgical instruments, such as cranial drill, scalpel, and forceps, were used to dissect the skull and meningeal layers to expose the cerebral cortex with a diameter of 2 mm. MMEC was inserted into the cerebral cortex, and MMEC electrodes of about 1 mm were implanted in the gray matter. Subsequently, MMEC continuously monitored potentiometric signals associated with K^+, Ca^{2+}, and Na^+ concentrations in the cerebral cortex (Fig. 1c) of anesthetized rats without electrical stimulation. Potentiometric

signals were calculated into corresponding K^+, Ca^{2+}, and Na^+ concentrations according to the potential–concentration standard curves obtained from the above in vivo tests. Figures 6e–6g show that MMEC-recorded ion concentrations in the brain tissue remained stable during the three-hour testing period, indicating that K^+, Ca^{2+}, and Na^+ levels in the brain tissue remained almost constant under anesthesia. The average MMEC-measured K^+, Ca^{2+}, and Na^+ concentrations in the brain during the three-hour recording period were analyzed, as shown in Fig. 6h. The intracerebral experiment validated the possibility of the MMEC system as a promising tool to monitor ion fluctuations in the brain besides the conventional method of electrical signal recording.

A customized circuit and terminal were designed to support the operation of the MMEC device for applications. Figure 6i shows the logic schematics of the MMEC system, including the working path of circuit modules. Figures 6j and 6k show the design of PCB, comprising the functional modules for signal acquisition, processing, and transmission, and the details of each component are described in Figs. S10–S17 (Supplementary Information). The circuit contained integrated modules such as the MCU and peripheral modules. The circuit was designed to realize the potentiometric recording of the three ion concentrations and support the signal processing and control of the whole system. The sensing circuit module comprised three parallel sets of the two-electrode sensing system capable of separately recording potentiometric signals of three types of ions. The sensing circuit module could also transmit signals to MCU after signal amplification between the input and output terminals. MCU sampled and converted the analog signals that the sensing circuit module transmitted through a 12-bit analog-to-digital converter to obtain the corresponding digital signals. MCU processed the data in the digital domain, transmitting them to the application in real time via a low-power Bluetooth module for wireless data transmission. The Bluetooth wireless data transmission served the small portable system to support the data transmission functions of MMEC devices. The entire circuit was powered by an external battery to realize a portable wearable system. The wireless data transmission and the custom development of the corresponding mobile application resulted in a more complete system, achieving the real-time display of data collected by the sensor for immediate signal feedback. Figure 6l shows the mobile terminal software interface of the MMEC-based semi-implantable device system. Figure 6m shows the integrated MMEC and customized PCB of the MMEC-based semi-implantable device system. To demonstrate that the as-designed circuit could effectively support the sensing function of MMEC, the response of MMEC in the detection of K^+, Ca^{2+}, and Na^+ in the in vitro solution was tested, where potentiometric signals were detected using either the designed circuit or the CHI 760E electrochemical workstation (Fig. 6n). For K^+ sensing, the K^+ concentration in DI water was increased from 0 to 1, 10, and 100 mmol/L. K^+ MSE connected to the CHI 760E electrochemical workstation effectively detected the increased potentiometric signal with increased K^+ concentration. K^+ MSE connected to PCB could also detect the increase in potentiometric signal associated with increased K^+ concentration. Signals obtained from PCB recordings were compared to those obtained from the electrochemical workstation after baseline calibration. Results showed a high degree of overlap between the signals recorded by PCB and those recorded by the electrochemical workstation, demonstrating that PCB could effectively support K^+ MSE. Similarly, when the Na^+ or Ca^{2+} concentration in the solution gradually increased from 0 to 1, 10, and 100 mmol/L, potentiometric signals recorded by MMEC connected to PCB also gradually increased and possessed a good overlap with signals recorded by the electrochemical workstation. These results demonstrated that the designed PCB could effectively support MMEC in collecting ion-related potentiometric signals.

Conclusions

This study developed an integrated MMEC-based semi-implantable device system capable of recording fluctuations in K^+, Ca^{2+}, and Na^+ concentrations in tissue environments over long periods for health monitoring and early complication diagnosis. The MMEC-based semi-implantable device system was sensitive to changes in K^+, Ca^{2+}, and Na^+ concentrations and could be used for ion monitoring in subcutaneous and intracranial tissues. The small effect of electrode surface area on the potentiometric sensing mechanism suggests that the use of tiny fiber-like electrodes for potentiometric sensing is feasible. In vitro studies demonstrated that the small-volume MMEC-based semi-implantable device system provided a wide range of linear responsiveness, good selectivity, and temporal stability for the three ion indicators. By monitoring ions in subcutaneous and intracranial tissues of rats, the MMEC-based semi-implantable device system could quantify K^+, Ca^{2+}, and Na^+ concentrations in a prolonged and stable manner, demonstrating the potential of the MMEC system for clinical applications. The above results demonstrated the potential of a wearable MMEC system to track ion concentrations in the body over time and monitor for disease complications. It enables prolonged in vivo monitoring and early diagnosis through the optimal integration of wearable bioelectronics and biocompatible multifunctional devices. Moreover, it could monitor and diagnose other systemic disease signals using the strategy proposed in this study, providing a basis for early and precise treatment. More importantly, the excellent biocompatibility, small size

of the sensing element, and ease of use of the MMEC-based semi-implantable device system allow the sensing device to be used in broader scenarios and sensing areas. This study demonstrated its potential for in vivo tissue ion detection and monitoring of other diseases.

Supplementary Information The online version contains supplementary material available at https://doi.org/10.1007/s42242-023-00262-2.

Acknowledgements The authors would like to acknowledge financial support from the National Key R&D Program of China (Nos. 2021YFF1200700 and 2021YFA0911100), the National Natural Science Foundation of China (Nos. T2225010, 32171399, and 32171456), the Fundamental Research Funds for the Central Universities, Sun Yat-Sen University (No. 22dfx02), and Pazhou Lab, Guangzhou (No. PZL2021KF0003). The authors also would like to thank the funding support from the Opening Project of Key Laboratory of Microelectronic Devices & Integrated Technology, Institute of Microelectronics, Chinese Academy of Sciences, and State Key Laboratory of Precision Measuring Technology and Instruments (No. pilab2211). QQOY would like to thank the China Postdoctoral Science Foundation (No. 2022M713645). JL would like to thank the National Natural Science Foundation of China (No. 62105380) and the China Postdoctoral Science Foundation (No. 2021M693686).

Author contributions SH, STZ, XX, and HJC conceived the concept, designed the work, and wrote the manuscript. SH, STZ, MYH, CJY, XSH, and ZJL performed experiments. SH, STZ, MYH, HJC, and XX performed statistical analyses of datasets. HJC and XX supervised the study. All authors discussed the results and assisted in the preparation of the manuscript.

Declarations

Conflict of interest XX is an associate editor for *Bio-Design and Manufacturing* and was not involved in the editorial review or the decision to publish this article. The authors declare that they have no conflict of interest.

Ethical approval The experimental protocols were approved by the Institutional Animal Care and Use Committee of Sun Yat-Sen University. All animals were handled according to the Guidelines for the Care and Use of Laboratory Animals of the Institutional Animal Care and Use Committee of Sun Yat-Sen University (Nos. SYSU-IACUC-2021-000022 and SYSU-IACUC-2022-000029).

References

1. Pang C, Lee C, Suh KY (2013) Recent advances in flexible sensors for wearable and implantable devices. J Appl Polym Sci 130(3):1429–1441. https://doi.org/10.1002/app.39461
2. Tat T, Libanori A, Au C et al (2021) Advances in triboelectric nanogenerators for biomedical sensing. Biosens Bioelectron 171:112714. https://doi.org/10.1016/j.bios.2020.112714
3. Lennon AM, Buchanan AH, Kinde I et al (2020) Feasibility of blood testing combined with PET-CT to screen for cancer and guide intervention. Science 369(6499):eabb9601. https://doi.org/10.1126/science.abb9601
4. Zhao F, Liu YD, Dong H et al (2020) An electrochemophysiological microarray for real-time monitoring and quantification of multiple ions in the brain of a freely moving rat. Angew Chem Int Ed Engl 59(26):10426–10430. https://doi.org/10.1002/anie.202002417
5. Teymourian H, Tehrani F, Mahato K et al (2021) Lab under the skin: microneedle based wearable devices. Adv Healthc Mater 10(17):e2002255. https://doi.org/10.1002/adhm.202002255
6. Zdrachek E, Bakker E (2021) Potentiometric sensing. Anal Chem 93(1):72–102. https://doi.org/10.1021/acs.analchem.8b04681
7. Wang F, Liu YJ, Zhang MD et al (2021) Home detection technique for Na^+ and K^+ in urine using a self-calibrated all-solid-state ion-selective electrode array based on polystyrene–Au ion-sensing nanocomposites. Anal Chem 93(23):8318–8325. https://doi.org/10.1021/acs.analchem.1c01203
8. Shao YZ, Ying YB, Ping JF (2020) Recent advances in solid-contact ion-selective electrodes: functional materials, transduction mechanisms, and development trends. Chem Soc Rev 49(13):4405–4465. https://doi.org/10.1039/C9CS00587K
9. Kuhlmann J, Witte F, Heineman WR (2013) Electrochemical sensing of dissolved hydrogen in aqueous solutions as a tool to monitor magnesium alloy corrosion. Electroanalysis 25(5):1105–1110. https://doi.org/10.1002/elan.201200457
10. Miller PR, Skoog SA, Edwards TL et al (2012) Hollow microneedle-based sensor for multiplexed transdermal electrochemical sensing. J Vis Exp 64:e4067. https://doi.org/10.3791/4067
11. Ma GJ, Wu CW (2017) Microneedle, bio-microneedle and bio-inspired microneedle: a review. J Contr Release 251:11–23. https://doi.org/10.1016/j.jconrel.2017.02.011
12. Luo HY, Lu YY, Xu YH et al (2022) A fully soft, self-powered vibration sensor by laser direct writing. Nano Energy 103:107803. https://doi.org/10.1016/j.nanoen.2022.107803
13. Yao SS, Zhu Y (2014) Wearable multifunctional sensors using printed stretchable conductors made of silver nanowires. Nanoscale 6(4):2345–2352. https://doi.org/10.1039/c3nr05496a
14. Parrilla M, Cuartero M, Crespo GA (2019) Wearable potentiometric ion sensors. TrAC Trends Anal Chem 110:303–320. https://doi.org/10.1016/j.trac.2018.11.024
15. Lu YY, Yang G, Shen YJ et al (2022) Multifunctional flexible humidity sensor systems towards noncontact wearable electronics. Nano-Micro Lett 14(1):150. https://doi.org/10.1007/s40820-022-00895-5
16. Ma Y, Zheng Q, Liu Y et al (2016) Self-powered, one-stop, and multifunctional implantable triboelectric active sensor for real-time biomedical monitoring. Nano Lett 16(10):6042–6051. https://doi.org/10.1021/acs.nanolett.6b01968
17. Zheng Q, Zhang H, Shi BJ et al (2016) In vivo self-powered wireless cardiac monitoring via implantable triboelectric nanogenerator. ACS Nano 10(7):6510–6518. https://doi.org/10.1021/acsnano.6b02693
18. Fang JR, Huang S, Liu FM et al (2022) Semi-implantable bioelectronics. Nano-Micro Lett 14(7):354–408. https://doi.org/10.1007/s40820-022-00818-4
19. Rodbard D (2016) Continuous glucose monitoring: a review of successes, challenges, and opportunities. Diabetes Technol Ther 18(S2):S23–S213. https://doi.org/10.1089/dia.2015.0417
20. Battelino T, Danne T, Bergenstal RM et al (2019) Clinical targets for continuous glucose monitoring data interpretation: recommendations from the international consensus on time in range. Diabetes Care 42(8):1593–1603. https://doi.org/10.2337/dci19-0028
21. Huang XH, Yang JB, Huang S et al (2022) Minimally invasive technology for continuous glucose monitoring. Bio-Des Manuf 5(1):9–13. https://doi.org/10.1007/s42242-021-00176-x
22. Shin H, Son Y, Chae U et al (2019) Multifunctional multi-shank neural probe for investigating and modulating long-range neural circuits in vivo. Nat Commun 10(1):3777. https://doi.org/10.1038/s41467-019-11628-5

23. Donoghue T, Haller M, Peterson EJ et al (2020) Parameterizing neural power spectra into periodic and aperiodic components. Nat Neurosci 23(12):1655–1665. https://doi.org/10.1038/s41593-020-00744-x
24. Van den Bergh BRH, van den Heuvel MI, Lahti M et al (2020) Prenatal developmental origins of behavior and mental health: the influence of maternal stress in pregnancy. Neurosci Biobehav Rev 117:26–64. https://doi.org/10.1016/j.neubiorev.2017.07.003
25. Kozai TD, Jaquins-Gerstl AS, Vazquez AL et al (2015) Brain tissue responses to neural implants impact signal sensitivity and intervention strategies. ACS Chem Neurosci 6(1):48–67. https://doi.org/10.1021/cn500256e
26. Liu ZQ, Liu JQ, Sun TC et al (2021) Integrated multiplex sensing bandage for in situ monitoring of early infected wounds. ACS Sens 6(8):3112–3124. https://doi.org/10.1021/acssensors.1c01279
27. Wang LY, Xie SJ, Wang ZY et al (2020) Functionalized helical fibre bundles of carbon nanotubes as electrochemical sensors for long-term in vivo monitoring of multiple disease biomarkers. Nat Biomed Eng 4(2):159–171. https://doi.org/10.1038/s41551-019-0462-8
28. Yang H, Qian ZY, Wang JJ et al (2022) Carbon nanotube array-based flexible multifunctional electrodes to record electrophysiology and ions on the cerebral cortex in real time. Adv Funct Mater 32(38):10. https://doi.org/10.1002/adfm.202204794
29. Mohan AMV, Windmiller JR, Mishra RK et al (2017) Continuous minimally-invasive alcohol monitoring using microneedle sensor arrays. Biosens Bioelectron 91:574–579. https://doi.org/10.1016/j.bios.2017.01.016
30. Gao W, Emaminejad S, Nyein HYY et al (2016) Fully integrated wearable sensor arrays for multiplexed in situ perspiration analysis. Nature 529(7587):509–514. https://doi.org/10.1038/nature16521
31. Xu H, Lu YF, Xiang JX et al (2018) A multifunctional wearable sensor based on a graphene/inverse opal cellulose film for simultaneous, in situ monitoring of human motion and sweat. Nanoscale 10(4):2090–2098. https://doi.org/10.1039/c7nr07225b
32. Huang XC, Li JY, Liu YM et al (2022) Epidermal self-powered sweat sensors for glucose and lactate monitoring. Bio-Des Manuf 5(1):201–209. https://doi.org/10.1007/s42242-021-00156-1
33. Heng WZ, Yang G, Kim WS et al (2022) Emerging wearable flexible sensors for sweat analysis. Bio-Des Manuf 5(1):64–84. https://doi.org/10.1007/s42242-021-00171-2
34. Urbanowicz M, Pijanowska DG, Jasiński A et al (2019) A miniaturized solid-contact potentiometric multisensor platform for determination of ionic profiles in human saliva. J Solid State Electr 23(12):3299–3308. https://doi.org/10.1007/s10008-019-04429-9
35. Cuartero M, Parrilla M, Crespo GA (2019) Wearable potentiometric sensors for medical applications. Sensors 19(2):363. https://doi.org/10.3390/s19020363
36. Li JH, Qin W (2020) An integrated all-solid-state screen-printed potentiometric sensor based on a three-dimensional self-assembled graphene aerogel. Microchem J 159:105453. https://doi.org/10.1016/j.microc.2020.105453
37. Lee H, Song C, Hong YS et al (2017) Wearable/disposable sweat-based glucose monitoring device with multistage transdermal drug delivery module. Sci Adv 3(3):e1601314. https://doi.org/10.1126/sciadv.1601314
38. Nyein HYY, Tai LC, Ngo QP et al (2018) A wearable microfluidic sensing patch for dynamic sweat secretion analysis. ACS Sens 3(5):944–952. https://doi.org/10.1021/acssensors.7b00961
39. Kim J, Sempionatto JR, Imani S et al (2018) Simultaneous monitoring of sweat and interstitial fluid using a single wearable biosensor platform. Adv Sci 5(10):1800880. https://doi.org/10.1002/advs.201800880
40. Lacour SP, Courtine G, Guck J (2016) Materials and technologies for soft implantable neuroprostheses. Nat Rev Mater 1(10):16063. https://doi.org/10.1038/natrevmats.2016.63
41. Yu W, Yao N, Pan J et al (2022) Highly sensitive and fast response strain sensor based on evanescently coupled micro/nanofibers. Opto Electron Adv 5(9):210101. https://doi.org/10.29026/oea.2022.210101
42. Rasmussen R, O'Donnell J, Ding FF et al (2020) Interstitial ions: a key regulator of state-dependent neural activity? Prog Neurobiol 193:101802. https://doi.org/10.1016/j.pneurobio.2020.101802
43. Li P, Lee GH, Kim SY et al (2021) From diagnosis to treatment: recent advances in patient-friendly biosensors and implantable devices. ACS Nano 15(2):1960–2004. https://doi.org/10.1021/acsnano.0c06688

Authors and Affiliations

Shuang Huang[1,2] · Shantao Zheng[1] · Mengyi He[1] · Chuanjie Yao[1] · Xinshuo Huang[1] · Zhengjie Liu[1] · Qiangqiang Ouyang[3] · Jing Liu[3] · Feifei Wu[1,4] · Hang Gao[5] · Xi Xie[1,2,3] · Hui-jiuan Chen[1]

✉ Xi Xie
xiexi27@mail.sysu.edu.cn

✉ Hui-jiuan Chen
chenhuix5@mail.sysu.edu.cn

[1] State Key Laboratory of Optoelectronic Materials and Technologies, Guangdong Province Key Laboratory of Display Material and Technology, School of Electronics and Information Technology, Sun Yat-Sen University, Guangzhou 510006, China

[2] Guangdong Provincial Key Laboratory of Sensor Technology and Biomedical Instrument, School of Biomedical Engineering, Sun Yat-Sen University, Shenzhen 518107, China

[3] The First Affiliated Hospital of Sun Yat-Sen University, Guangzhou 510080, China

[4] Pazhou Lab, Guangzhou 510335, China

[5] Institute of Microelectronics of the Chinese Academy of Sciences, Beijing 100029, China